

High-throughput screening of metal-porphyrin-like graphenes for selective capture of carbon dioxide

**Hyeonhu Bae^{1,†}, Minwoo Park^{1,†}, Byungryul Jang¹, Yura Kang², Jinwoo Park²,
Hosik Lee³, Haegeun Chung⁴, ChiHye Chung⁵, Suklyun Hong², Yongkyung Kwon¹,
Boris I. Yakobson⁶, Hoonkyung Lee^{1,*}**

¹School of Physics, Konkuk University, Seoul 143-701, Korea

²Department of Physics and Graphene Research Institute, Sejong University, Seoul 143-747, Korea

³School of Mechanical and Advanced Materials Engineering, Ulsan National Institute of Science and Technology, Ulsan 689-798, Korea

⁴Department of Environmental Engineering, Konkuk University, Seoul 143-701, Korea

⁵Department of Biological Sciences, Konkuk University, Seoul 143-701, Korea

⁶Department of Materials Science and Nanoengineering, Rice University, Houston, Texas 77005, United State

[†]These authors contributed equally to this work.

Number of pages: 24

Correspondence to Hoonkyung Lee; correspondence and requests for materials should be addressed to H. L. (Email: hkiee3@konkuk.ac.kr).

Nanostructured materials, such as zeolites and metal-organic frameworks, have been considered to capture CO₂. However, their application has been limited largely because they exhibit poor selectivity for flue gases and low capture capacity under low pressures. We perform a high-throughput screening for selective CO₂ capture from flue gases by using first principles thermodynamics. We find that elements with empty *d* orbitals selectively attract CO₂ from gaseous mixtures under low CO₂ pressures ($\sim 10^{-3}$ bar) at 300 K and release it at ~ 450 K. CO₂ binding to elements involves hybridization of the metal *d* orbitals with the CO₂ π orbitals and CO₂-transition metal complexes were observed in experiments. This result allows us to perform high-throughput screening to discover novel promising CO₂ capture materials with empty *d* orbitals (e.g., Sc- or V-porphyrin-like graphene) and predict their capture performance under various conditions. Moreover, these findings provide physical insights into selective CO₂ capture and open a new path to explore CO₂ capture materials.

Carbon dioxide gas is a greenhouse gas that is a primary cause of global warming, which is known to cause severe climate change¹. In recent years, the temperature of the earth has increased because of significant increase in CO₂ emission. The emission of this gas is expected to continuously increase as the demand for fossil fuels increases, and thus the development of technologies for CO₂ capture is essential for addressing climate change¹. The technology involving the capture of CO₂ gas from the flue gas is currently not sufficiently developed, particularly in the backdrop of the urgent need to reduce CO₂ emission.

Nanostructured materials, such as graphene, zeolites, and metal-organic frameworks, have been considered to capture CO₂. These materials are potentially useful because of their high capacity, fast CO₂ adsorption kinetics, and effective regeneration²⁻¹¹. However, their application has been limited largely because they exhibit poor selectivity for flue gases and low capture capacity under low pressures ($\sim 10^{-3}$ bar)¹¹⁻¹⁴, thereby limiting CO₂ capture from flue gases in power plants¹⁴. Thus, there is an increasing demand to search for novel CO₂ capture materials¹⁵⁻¹⁷.

Recently, Fe–porphyrin-like fragments (FeN₄) to carbon nanotubes¹⁸ and Co–porphyrin-like fragments (CoN₄) to nanostructures¹⁹ were synthesized using the chemical vapour deposition and the pyrolysis methods, respectively, where Fe or Co is located at the center of four nitrogen atoms similar to metal-porphyrin structure^{20,21}. We herein refer to this MN₄ structure as an M–porphyrin-like structure. Computational studies have shown that transition metal (TM)–porphyrin-like graphenes are stable^{22,23}. Fused TM–porphyrin-like nanoclusters have been synthesized experimentally^{20,21,24-28}. Furthermore, the porphyrin-like structure is analogous to the local structure of Fe in hemoglobin²⁹ or myoglobin³⁰, which deliver O₂ to the organs in the body. The concentration of nitrogen in carbon nanotubes and graphene has been found to reach $\sim 8\%$ ³¹ and $\sim 10\%$ ³², respectively. Thus, we expect that TM–porphyrin-like nanostructures can be synthesized experimentally. In this article, we perform first-principles thermodynamics based high-throughput screening for suitable M elements as selective CO₂ attractors using M–porphyrin-like graphene.

Results

To measure the CO₂ capture capabilities of nanomaterials from a mixed gas, we constructed a thermodynamic model of CO₂ adsorption on an adsorbent using the grand-canonical partition function³³. We assumed a surface containing the number of identical, independent, and distinguishable adsorption sites (N_s) with no mixed adsorption of different molecules per adsorption site, wherein the number of adsorbed i -type gas molecules on the surface is N_i . If the adsorbed molecules and gases are in equilibrium, the grand partition function of the system can be written as

$$Z = (1 + \sum_i \sum_{n_i=1} g_{n_i} e^{n_i(\mu^i - \varepsilon_{n_i}^i)/k_B T})^{N_s}, \quad (1)$$

where superscript i indicates the type of gas, $\mu^i (< 0)$ denotes the chemical potential of the i -type gas, and $\varepsilon_{n_i}^i (< 0)$ and g_{n_i} denote the average adsorption energy and degeneracy of configuration (for a given adsorption number n_i) of the i -type gas molecules, respectively. When the thermally average number of i -type CO₂ is calculated from $\langle N_i \rangle = k_B T \partial \ln Z / \partial \mu^i$, the occupation function (i.e., coverage) of CO₂ for an adsorption site can be written as

$$f_{\text{CO}_2}(P, T) \equiv \frac{\langle N_{\text{CO}_2} \rangle}{N_s} = \frac{\sum_{n_{\text{CO}_2}=1} n_{\text{CO}_2} g_{n_{\text{CO}_2}} e^{n_{\text{CO}_2}(\mu^{\text{CO}_2} - \varepsilon_{n_{\text{CO}_2}}^{\text{CO}_2})/k_B T}}{1 + \sum_i \sum_{n_i=1} g_{n_i} e^{n_i(\mu^i - \varepsilon_{n_i}^i)/k_B T}}, \quad (2)$$

Therefore, the thermodynamic CO₂ capture capacity of nanomaterials from a mixed gas can be computed using

$$C(P, T) = N_s f_{\text{CO}_2}(P, T) / \sum_i M_i m_i, \quad (3)$$

where M_i and m_i denote the atomic mass and number of elements comprising the adsorbent, respectively.

The occupation function of CO₂ would have a positive value, i.e., $f_{\text{CO}_2} > 0$, if $\mu^{\text{CO}_2}(300\text{K}) > \varepsilon^{\text{CO}_2}$ and $\Delta^{\text{CO}_2} > \Delta^{\text{other}}$ at the adsorption (capture) conditions as shown in Figure 1a, wherein $\Delta^i \equiv \mu^i - \varepsilon^i$ is set and the superscript 'other' denotes molecules other than CO₂. In this case, selective CO₂ adsorption occurs through competitive adsorption between CO₂ and other molecules; this is attributed to the fact that the Gibbs factor for CO₂ adsorption is much greater than unity and the Gibbs factors of other molecules, i.e., $e^{(\mu^{\text{CO}_2} - \varepsilon^{\text{CO}_2})/k_B T} \gg 1$ and $e^{(\mu^{\text{CO}_2} - \varepsilon^{\text{CO}_2})/k_B T} \gg e^{(\mu^{\text{other}} - \varepsilon^{\text{other}})/k_B T}$. However, the occupation function would be zero, i.e., $f_{\text{CO}_2} = 0$, if $\mu^{\text{CO}_2}(450\text{K}) < \varepsilon^{\text{CO}_2}$, at the desorption (release) conditions ($e^{(\mu^{\text{CO}_2} - \varepsilon^{\text{CO}_2})/k_B T} \ll 1$) as shown in Figure 1b, indicating that CO₂ adsorbed on the metal sites is released. Under a CO₂ pressure of $\sim 10^{-3}$ bar, the ideal conditions for adsorption and desorption are assumed to be 300 and 450 K, respectively, where μ^{CO_2} is approximately -0.75 and -1.20 eV, respectively, at ambient conditions. Thus, the key thermodynamic conditions for reversible and selective CO₂ capture from a mixed gas are as follows: (i) $-1.20 \text{ eV} < \varepsilon^{\text{CO}_2} < -0.75 \text{ eV}$ and (ii) $\Delta^{\text{CO}_2} > \Delta^{\text{other}}$.

From this we construct a computational approach to efficiently predict selective CO₂ capture materials based on first principles thermodynamics shown in Fig. 1(c). The thermodynamic conditions and capacity requirements¹¹ for screening are as follows: $-1.20 \text{ eV} < \varepsilon^{\text{CO}_2} < -0.75 \text{ eV}$ and $\Delta C(P,T) > 3 \text{ mmol g}^{-1}$ for CO₂ gas, and $\Delta^{\text{CO}_2} > \Delta^{\text{other}}$ and $\Delta C(P,T) > 3 \text{ mmol g}^{-1}$ for a mixed gas. $\Delta C(P,T)$ denotes the difference between $C(P,T)$ at 300 K and $C(P,T)$ at 450 K under a pressure of 10^{-3} bar, which indicates the CO₂ working capacity. These requirements may need to be revised depending on the operational environments.

We performed calculations on the adsorption energy of CO₂ molecules on the M sites of M–porphyrin-like graphene (Figure 2a). Elements of atomic numbers up to 92 for the M site were considered, and the others were ruled out because of their heavy weight. Sc–, V–, Tc–, Os–, and Th–porphyrin-like graphenes out of many candidates met the reversibility requirements, viz. -1.2 to -0.8 eV (Figure 2a), where a CO₂ molecule adsorbs on a TM atom with the distance of ~ 2.5 Å between the TM atom and the CO₂ molecule. Therefore they were considered for the next step. We also performed CO₂ adsorption calculations on carbon allotropes such as carbon nanotubes, graphene, and C₆₀. The adsorption energy of the CO₂ molecule is ca. -0.05 eV, and the distance between their surface and the molecules is ~ 3.5 Å. In this case, since the adsorption energy of CO₂ molecules is much smaller than the required adsorption energy, pristine carbon nanostructures may not be suitable for use as CO₂ capture media under low pressure at room temperature. Notably, our approach significantly reduces the computational load because it is not necessary to calculate $\Delta C(P,T)$ for all the candidates in CO₂ gas or a mixed gas.

To predict the capture capabilities of the candidates, the CO₂ working capacities, $\Delta C(P,T)$, of the structures were computed using Eq. (3) (Figure 2b). The experimental values of the chemical potentials of CO₂ gas²² and calculated adsorption energies ($\epsilon_n^{\text{CO}_2}$) were used in these calculations. Since the working capacities of Sc–, V–, and Tc–porphyrin-like graphenes satisfied the capacity requirement (>3 mmol g⁻¹), they were considered for the next selectivity screening step.

We observed three different geometries for the adsorbed CO₂ molecules on the TM atoms, which were designated as η^1 -CO₂, η^2 -CO₂, and η^3 -CO₂, corresponding to the coordination numbers of the TM atom, i.e., 1, 2, and 3, respectively (Figure 3a). The adsorption energies of the CO₂ molecules were calculated to be -0.54, -0.79, and -0.78 eV per CO₂ for the Sc- η^1 -CO₂, Sc- η^2 -CO₂, and Sc- η^3 -CO₂ geometries, respectively. The preferred CO₂ geometry depends on the metal type. The distance between the CO₂ molecule and TM atoms is 2.2–2.5 Å, which is much smaller than the equilibrium van der Waals distance (~3.4 Å), and the bond lengths of CO₂ are elongated by ~5%. Thus, the bonding between the TM atoms and CO₂ molecules must be chemical in nature.

To understand the enhanced interaction between early *d* orbital-containing elements and CO₂ molecules, we focused on a binding mechanism that appears between TM atoms and olefin molecules and is well known in organometallic chemistry²³. The Dewar–Chatt–Duncanson model explains the type of chemical bonding between a π -orbital acid alkene and *d*-orbital metal atom by electron donation (i.e., hybridization of the empty *d* states with filled π states) and back-donation (i.e., hybridization of the filled *d* states with empty π states)²³. The interaction between the TM *d* orbitals and the olefin π orbitals is called the “Dewar interaction”. Therefore, empty *d*-orbital metals are expected to attract CO₂ molecules. The Dewar interaction is based on chemical bonding between the TM and CO₂ and can enhance the strength of the M–CO₂ bond beyond that of the van der Waals interaction. It is noteworthy that Ca²⁺ also has empty 3*d* orbitals near the Fermi level that could participate in the Dewar interaction.

Next, we investigated whether the enhanced adsorption observed with early TM atoms is caused by the Dewar interaction. We observed the hybridization of the Sc 3*d* states

with the CO₂ states at around -2.5, -2.0, and -2.0 eV for the η^1 -CO₂, η^2 -CO₂, and η^3 -CO₂ geometries, respectively (Figure 3b). The difference in charge density between the Sc atom and CO₂ molecule (Figure 3c) indicates chemical bonding between CO₂ and the metal atoms. From this, we concluded that the enhanced binding of CO₂ to the metal atom originates from the Dewar interaction. The distinct adsorption geometries of CO₂ can be explained by the different hybridization states of the TM *d* orbitals with the CO₂ π orbitals (Figure 3d).

To examine the selectivity of CO₂ adsorption on Sc, V, and Tc sites in the presence of a mixed gas, we also carried out calculations on the adsorption of multiple CO₂ molecules or ambient gas molecules such as N₂, CH₄, and H₂ onto the metal atoms. Several CO₂, H₂, N₂, and CH₄ molecules bound to Sc, V, and Tc atoms (Figures. 4a and 4b, Figure 5). The difference between the chemical potential at 300 K and 10⁻³ bar and the adsorption energy of CO₂ (or other gas molecules) was calculated (Figure 4c) using experimental values³³ of the chemical potentials of CO₂, H₂, N₂, and CH₄ gases. The chemical potentials of gases were obtained by fitting the experimental values to the following expression $\mu^i(P,T) = \mu_{\text{ideal}}^i(P,T) + A^i + B^i \times T$ where upper subscript *i* indicates the type of gases, $\mu_{\text{ideal}}^i(P,T)$ denotes the chemical potential of an ideal monatomic *i*-type gas for a given the pressure *P* and the temperature *T*, and *A*^{*i*} and *B*^{*i*} are fitted coefficients of *i*-type gas. The fitted coefficients are presented in Table 1. Since Sc and V, and not Tc, were found to satisfy the conditions for selective CO₂ adsorption ($\Delta^{\text{CO}_2} > \Delta^{\text{other}}$), they were considered for the next screening step

We also considered the zero-point vibrational energy of the gas molecules adsorbed onto the TM atoms. This energy was calculated to be in the order of a few meV regardless of the metal. Since the zero-point vibrational energy is negligible compared to the (static) adsorption energy (Figure 4a), we ignored the influence of the zero-point vibrational energy on adsorption in all cases except for H₂. Since the zero-point energy of the H₂ molecules adsorbed on TM atoms was not negligible (25% of the calculated values), we corrected the H₂ adsorption energies to determine the true adsorption energy.

The statistical model obtained here can correctly describe the adsorption of CO₂ onto TM–porphyrin-like graphene in the presence of a mixed gas because the mixed adsorption of different molecules onto a TM atom is not energetically favorable. For instance, the adsorption energy at which both a CO₂ and N₂ molecule adsorb onto a Sc atom was calculated to be -0.9 eV, which is much higher than that (-1.3 eV) at which single CO₂ or N₂ molecules adsorb on different sites.

The CO₂ capture capacities, $C(P,T)$, from mixed gases with different compositions were calculated for Sc– and V–porphyrin-like graphenes (Figures. 6a and 6b). The ratios of the mixed gases were based on experimental measurements^{4,34} from pre-combustion, post-combustion, and oxyfuel-combustion CO₂ capture. These results show high CO₂ selectivity of Sc– and V–porphyrin-like graphene in mixed gases, which is consistent with the prediction of the selectivity requirement of $\Delta^{CO_2} > \Delta^{other}$. The CO₂ working capacities, $\Delta C(P,T)$, of Sc– and V–porphyrin-like graphenes can reach ~4 mmol g⁻¹ (Figures 6c and 6d), which meets the capacity requirement of 3 mmol g⁻¹ in a mixed gas. Therefore, Sc– and V–porphyrin-like graphene were found to be suitable for highly

selective CO₂ capture from flue gases at ambient conditions. Furthermore, the CO₂ pressure range covers the pressure ($\sim 0.4 \times 10^{-3}$ bar) of CO₂ in the atmosphere because the concentration of CO₂ in the atmosphere is ~ 400 ppm.

Discussion

We performed first-principles total energy calculations regarding CO₂ adsorption onto metal–porphyrin-like structures to explore the feasibility of achieving room-temperature CO₂ capture under low pressures. We found that transition metal–porphyrin-like structures adsorb CO₂ molecules with the desirable binding energy range and the practical (usable) capacity under ambient conditions can reach ~ 3 mmol/g. Equilibrium thermodynamics studies showed that Sc– or V–porphyrin-like graphene structures were found to be suitable for use as room-temperature CO₂ capture media. These results indicate that nanostructures containing empty *d* orbitals may be applied for selective adsorption of CO₂ from flue gases. We believe our results provide a new approach to achieving CO₂ capture at room temperature.

We address the evidence of CO₂ binding to TM atoms for CO₂ capture. TM- η^1 -CO₂ or TM- η^2 -CO₂ complexes were observed in experiments^{35,36}. The capture of CO₂ involved in the first step of carbon capture/storage (CCS) technology requires high energy consumption^{37,38}. Thus, the development of media such as TM–porphyrin-like graphene nanostructures, which can selectively adsorb CO₂ at room temperature under low CO₂ partial pressure, is expected to lower the cost of CO₂ adsorption and make CCS more viable.

Methods

We performed first-principles calculations based on the density functional theory (DFT)³⁹ as implemented in the Vienna Ab-initio Simulation Package (VASP) with the projector augmented wave (PAW) method⁴⁰. The generalized gradient approximation (GGA) in the Perdew–Burke–Ernzerhof scheme⁴¹ was used for the exchange correlation energy functional, and the kinetic energy cutoff was taken to be 800 eV. For calculations of gas molecule adsorption, our model for the graphene-based system comprised a 3×3 hexagonal supercell, and the composition of the supercell was $C_{12}N_4M_1$. Geometrical optimization of the graphene-based system was carried out until the Hellmann–Feynman force acting on each atom was less than 0.01 eV/\AA . The first Brillouin zone integration was performed using the Monkhorst–Pack scheme⁴². 4×4 k-point sampling was used for the 3×3 graphene supercells.

REFERENCES

- (1) Stocker, T. F., Ed. *Climate Change 2013: The Physical Science Basis. Contribution of Working Group I to the Fifth Assessment Report of the Intergovernmental Panel on Climate Change* (Cambridge Univ. Press, London), 2013.
- (2) Liu, Y., Wang, Z. U. and Zhou, H. –C. Recent advances in carbon dioxide capture with metal-organic frameworks. *Greenhouse Gas. Sci. Technol.* **2**, 239 (2012)
- (3) Cinke, M., Li, J., Bauschlicher, C. W., Ricca, A. and Meyyappan, M. CO₂ adsorption in single-walled carbon nanotubes. *Chem. Phys. Lett.* **376**, 761 (2011)
- (4) Sumida, K. et al. Carbon dioxide capture in metal-organic frameworks. *Chem. Rev.* **112**, 724 (2012)

- (5) Wang, B., Côté, A. P., Furukawa, H., O’Keeffe, M. and Yaghi, O. M. Colossal cages in zeolitic imidazole frameworks as selective carbon dioxide reservoirs. *Nature* **453**, 207 (2008)
- (6) Bezerra, D. P., Oliveira, R. S., Vieira, R. S., Cavalcante, C. L. and Azevedo, D. S. C. Adsorption of CO₂ on nitrogen-enriched activated carbon and zeolite 13X. *Adsorption* **17**, 235 (2011)
- (7) Furukawa, H. et al. Ultrahigh porosity in metal-organic frameworks. *Science* **329**, 424 (2010)
- (8) Sun, W. et al. High surface area tunnels in hexagonal WO₃. *Nano Lett.* **15**, 4834 (2015)
- (9) Kondo A. et al. Novel expansion/shrinkage modulation of 2D layered MOF triggered by clathrate formation with CO₂ molecules. *Nano Lett.* **6**, 2581 (2006)
- (10) Kim, S., Jinschek, J. R., Chen, H., Sholl, D. S. and Marand, E. Scalable fabrication of carbon nanotube/polymer nanocomposite membranes for high flux gas transport. *Nano Lett.* **7**, 2806 (2007)
- (11) Samanta, A., Zhao, A., Shimizu, G. K. H., Sarkar, P. and Gupta, R. Post-combustion CO₂ capture using solid sorbents: a review. *Ind. Eng. Chem. Res.* **51**, 1438 (2012)
- (12) Lin, L. –C. et al. In silico screening of carbon-capture materials. *Nat. Mat.* **2012**, *11*, 633.
- (13) Liu, H. et al. A hybrid absorption-adsorption method to efficiently capture carbon. *Nat. Commun.* **5**, 5147 (2014)
- (14) Xiang, S. et al. Microporous metal-organic framework with potential for carbon dioxide capture at ambient conditions. *Nat. Commun.* **3**, 954 (2012)
- (15) Oh, J. et al. Borane-modified graphene-based materials as CO₂ adsorbents. *Carbon* **79**, 450 (2014)
- (16) Choi, H., Park, Y. C., Kim, Y. –H. and Lee, Y. S. Ambient carbon dioxide capture by boron-rich boron nitride nanotube. *J. Am. Chem. Soc.* **133**, 2084 (2011)

- (17) Sun, Q., Wang, M., Li, Z., Du, A. and Searles, D. J. Carbon dioxide capture and gas separation on B₈₀ fullerene. *J. Phys. Chem. C* **118**, 2170 (2014)
- (18) Lee, D. H., Lee, W. J., Lee, W. J., Kim, S. O. and Kim, Y. -H. Theory, synthesis, and oxygen reduction catalysis of Fe-porphyrin-like carbon nanotube. *Phys. Rev. Lett.* **106**, 175502 (2011)
- (19) Liang, H. -W. et al. Molecular metal-N_x centres in porous carbon for electrocatalytic hydrogen evolution. *Nat. Commun.* **6**, 7992 (2015)
- (20) Tsuda, A., Furuta, H. and Osuka, A. Synthesis, structural characterizations, and optical and electrochemical properties of directly fused diporphyrins. *J. Am. Chem. Soc.* **123**, 10304 (2011)
- (21) Tsuda, A., Furuta, H. and Osuka, A. Completely fused diporphyrins and triporphyrin. *Angew. Chem. Int. Ed.* **39**, 2549 (2000)
- (22) The chemical potential of gases, $\mu = (H - TS)/N$, where H , S , and N denote the enthalpy, the entropy, and the number of particles was calculated from the data of the enthalpy (H) and entropy (S) in the reference: <http://webbook.nist.gov/chemistry/fluid/>.
- (23) Michael, D. and Mingos, P. A historical perspective on Dewar's landmark contribution to organometallic chemistry. *J. Organomet. Chem.* **635**, 1 (2001)
- (24) Aratani, N., Osuka, A., Cho, H. S. and Kim, D. Photochemistry of covalently-linked multi-porphyrinic systems. *J. Photochem. Photobiol. C* **3**, 25 (2001)
- (25) Kim, K. S., Lim, J. M., Osuka, A. and Kim, D. Various strategies for highly-efficient two-photon absorption in porphyrin arrays. *J. Photochem. Photobiol. C* **9**, 13 (2008)
- (26) Tanaka, T. et al. Synthesis and properties of hybrid porphyrin tapes. *Chem. Eur. J.* **17**, 14400 (2011)
- (27) Tanaka, S. et al. Toward ultralow-bandgap liquid crystalline semiconductors: use of triply fused metalloporphyrin trimer-pentamer as extra-large π -extended mesogenic motifs. *Chem. Eur. J.* **18**, 10554 (2012)

- (28) Nakamura, Y. et al. A directly fused tetrameric porphyrin sheet and its anomalous electronic properties that arise from the planar cyclooctatetraene core. *J. Am. Chem. Soc.* **128**, 4119 (2006)
- (29) Perutz, M. F. et al. Structure of haemoglobin: a three-dimensional Fourier synthesis at 5.5-Å. resolution. *Nature* **185**, 416 (1960)
- (30) Kendrew, J. C. et al. Structure of myoglobin: a three-dimensional Fourier synthesis at 2 Å. resolution. *Nature* **185**, 422 (1960)
- (31) Lee, D. H., Lee, W. J. and Kim, S. O. Highly efficient vertical growth of wall-number-selected, N-doped carbon nanotube arrays. *Nano Lett.* **9**, 1427 (2009)
- (32) Sun, Y. et al. Chemically converted graphene as substrate for immobilizing and enhancing the activity of a polymeric catalyst. *Chem. Commun.* **46**, 4740 (2010)
- (33) Kittel, C. and Kroemer, H. *Thermal Physics*, 140-143 (W. H. Freeman & Company: New York), 1980
- (34) Kakaras, E., Koumanakos, A., Doukelis, A., Ginnakopoulos, D. and Vorrias, I. Oxyfuel boiler design in a lignite-fired power plant. *Fuel* **86**, 2144 (2007)
- (35) Calabrese, J. C., Herskovitz, T. and Kinney, J. B. Carbon dioxide coordination chemistry 5. the preparation and structure of the rodium complex Rh(eta.1-CO₂)(Cl)(diars)₂. *J. Am. Chem. Soc.* **105**, 5914 (1983)
- (36) Pandey, K. K. Reactivities of carbonyl sulfide (COS), carbon disulfide (CS₂) and carbon dioxide (CO₂) with transition metal complexes. *Coord. Chem. Rev.* **140**, 37 (1995)
- (37) Haszeldine, R. S. Carbon capture and storage: how green can black be? *Science*, **325**, 1647 (2009)
- (38) Steeneveldt, R., Berger, B. and Torp, T. A. CO₂ capture and storage: closing the knowing-doing gap. *Chem. Eng. Res. Des.* **84**, 739 (2006)

- (39) Kohn, W. and Sham, L. Self-consistent equations including exchange and correlation effects. *J. Phys. Rev.* **140**, A1133 (1965)
- (40) Kresse, G. and Joubert, D. From ultrasoft pseudopotentials to the projector augmented-wave method. *Phys. Rev. B* **59**, 1758 (1999)
- (41) Perdew, J. P., Burke, K. and Ernzerhof, M. Generalized gradient approximation made simple. *Phys. Rev. Lett.* **77**, 3865 (1996)
- (42) Monkhorst, H. J. and Pack, J. D. Special points for Brillouin-zone integrations. *Phys. Rev. B* **13**, 5188 (1976)

Acknowledgments

We thank C. H. Park for critical reading. This research was supported by WTU Joint Research Grants of Konkuk University, the Basic Science Research Program (H. L.^a: 2015R1A1A1A05001583), and Nano-Material Technology Development Program (S. H.: 2012M3A7B4049888) through the National Research Foundation of Korea (NRF) funded by the Ministry of Science, ICT & Future Planning. The Priority Research Center Program (S. H.:2010-0020207) through NRF funded by the Ministry of Education (MOE) also supported this work.

Author Contributions

H. B., B. J., and M. P. contributed equally to this work. H.L.^a conceived and designed the study. H. B., B. J., M. P., and J. P. performed the calculations. Y. K.^a, H. L.^b, C. H., C. C., S. H., Y. K.^b, and H. L. interpreted the data. C. C. and H. L.^a wrote the manuscript. All authors revised the manuscript and approved the final version of the manuscript.

Author Information

Supplementary information is available in the online version of the paper. Reprints and permissions information is available at www.nature.com/reprints. Correspondence and requests for materials should be addressed to H. L.^a (hkiee3@konkuk.ac.kr).

Competing Financial Interests

The authors declare no competing financial interests.

Table 1. The fitted chemical potentials of gases.

| Gas type | A^i (eV) | B^i (eV/K) | R^2 |
|-----------------|------------------------------|--------------------------------|-------------------------|
| CO ₂ | 0.04271 | -0.6425 | 0.99882 |
| H ₂ | 0.02784 | -0.1585 | 0.99590 |
| N ₂ | 0.03000 | -0.4512 | 0.99948 |
| CH ₄ | 0.04868 | -0.4840 | 0.99823 |

R^2 is the coefficient of determination (measure of goodness of fit).

Figures legends

Figure 1. Thermodynamics of reversible/selective adsorption of CO₂ and flow chart for predicting selective CO₂ capture materials: (a) Selective CO₂ adsorption occurs through competitive adsorption between CO₂ and other molecules if $\mu^{\text{CO}_2}(300\text{ K}) > \varepsilon^{\text{CO}_2}$ and $\Delta^{\text{CO}_2} > \Delta^{\text{other}}$. (b) CO₂ molecules adsorbed on the metal sites are released if $\mu^{\text{CO}_2}(450\text{ K}) < \varepsilon^{\text{CO}_2}$. (c) Flow chart for predicting reversible and selective CO₂ capture materials based on first principles thermodynamics: this consists of reversibility screening for pure CO₂ gas and selectivity screening for a mixed gas.

Figure 2. Reversibility screening of many candidates: (a) Calculated adsorption energies of CO₂ molecules on M–porphyrin-like graphene and a variety of nanostructures. Inset shows the schematic of CO₂ binding to the M site and colored-marked elements indicate data not available. (b) Calculated CO₂ capture capacity, $C(P,T)$, on M–porphyrin-like graphene for CO₂ gas at 300 K under a CO₂ pressure of 10⁻³ bar. Colored-marked bars indicate candidates which meet the requirements.

Figure 3. Origin of distinct geometries of CO₂ adsorption: (a) Atomic structures showing CO₂ molecule adsorbed onto Sc–4N graphene for the various CO₂ adsorption geometries designated as η^1 -CO₂, η^2 -CO₂, and η^3 -CO₂, respectively. (b) The density of states for η^1 , η^2 , and η^3 geometries, respectively. (c) The difference in the total charge density $\Delta\rho = \rho(\text{GP}+4\text{N}+\text{Sc}+\text{CO}_2) - \rho(\text{GP}+4\text{N}+\text{Sc}) - \rho(\text{CO}_2)$ for η^1 , η^2 , and η^3 geometries, respectively. Yellow and green indicates the charge accumulation and depletion. (d) The schematic of the hybridization of the Sc 3d orbitals with the CO₂ p_z orbitals for η^1 , η^2 , and η^3 geometries, respectively. Red and blue colors of the orbitals indicate the different phases, respectively.

Figure 4. Selectivity screening by selective CO₂ capture condition: (a) Calculated (average) adsorption energies of molecules for the different types of molecules with different numbers of the molecules as TM atoms (TM = Sc, V, Tc). *, **, and *** indicate the geometric configurations of η^1 , η^2 , and η^3 , respectively. (b) Optimized geometry of three CO₂ molecules adsorbed onto a Sc atom of Sc-porphyrin-like graphene with the η^1 configuration. (c) The difference ($\Delta^i = (\mu^i - \varepsilon_{n_i}^i)n_i$) between the chemical potential of a gas and adsorption energy of the gas molecule on TM-porphyrin-like graphene with respect to the type of gas. The largest values of Δ^i were chosen regardless of n_i .

Figure 5. Adsorption of various molecules on Sc-porphyrin-like graphene: (a) Up to three H₂ molecules adsorb on a Sc atom. (b) Up to three N₂ molecules adsorb on a Sc atom. (c) Up to two CH₄ molecules adsorb on a Sc atom.

Figure 6. Selectivity screening by CO₂ working capacity: Calculated capacities, $C(P,T)$, of CO₂ of the TM-porphyrin-like graphenes as a function of temperature under total pressure, P , of 10^{-3} bar using Eq. (3): (a) Sc-porphyrin-like graphene and (b) V-porphyrin-like graphene. The following different compositions of gases were considered: Pure CO₂ (100%), CO₂ (89%)-N₂ (11%), CO₂ (40%)-H₂ (57%)-N₂ (3%), CO₂ (20%)-H₂ (75%)-CH₄ (5%), and CO₂ (17%)-N₂ (83%). The partial pressure of gases is given by $P_i = x_i P$, where x_i is the composition of the gas. Calculated working capacities of CO₂ in the TM-porphyrin-like graphene as a function of the total pressure, P , of the gases from $\Delta C(P,T)$, the difference between $C(P,T)$ at 300 K and $C(P,T)$ at 450 K: (c) Sc-porphyrin-like graphene and (d) V-porphyrin-like graphene.

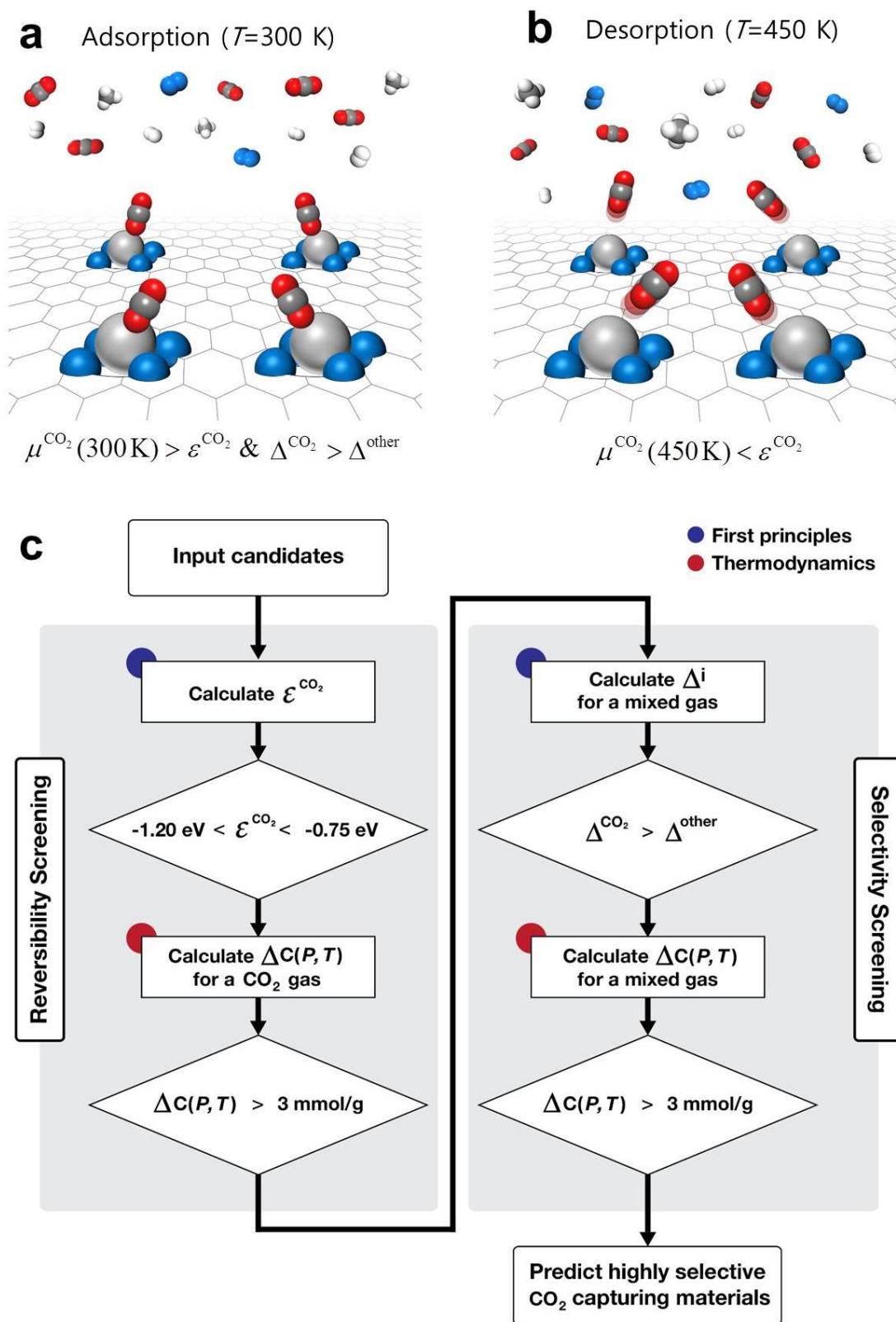


Figure 1

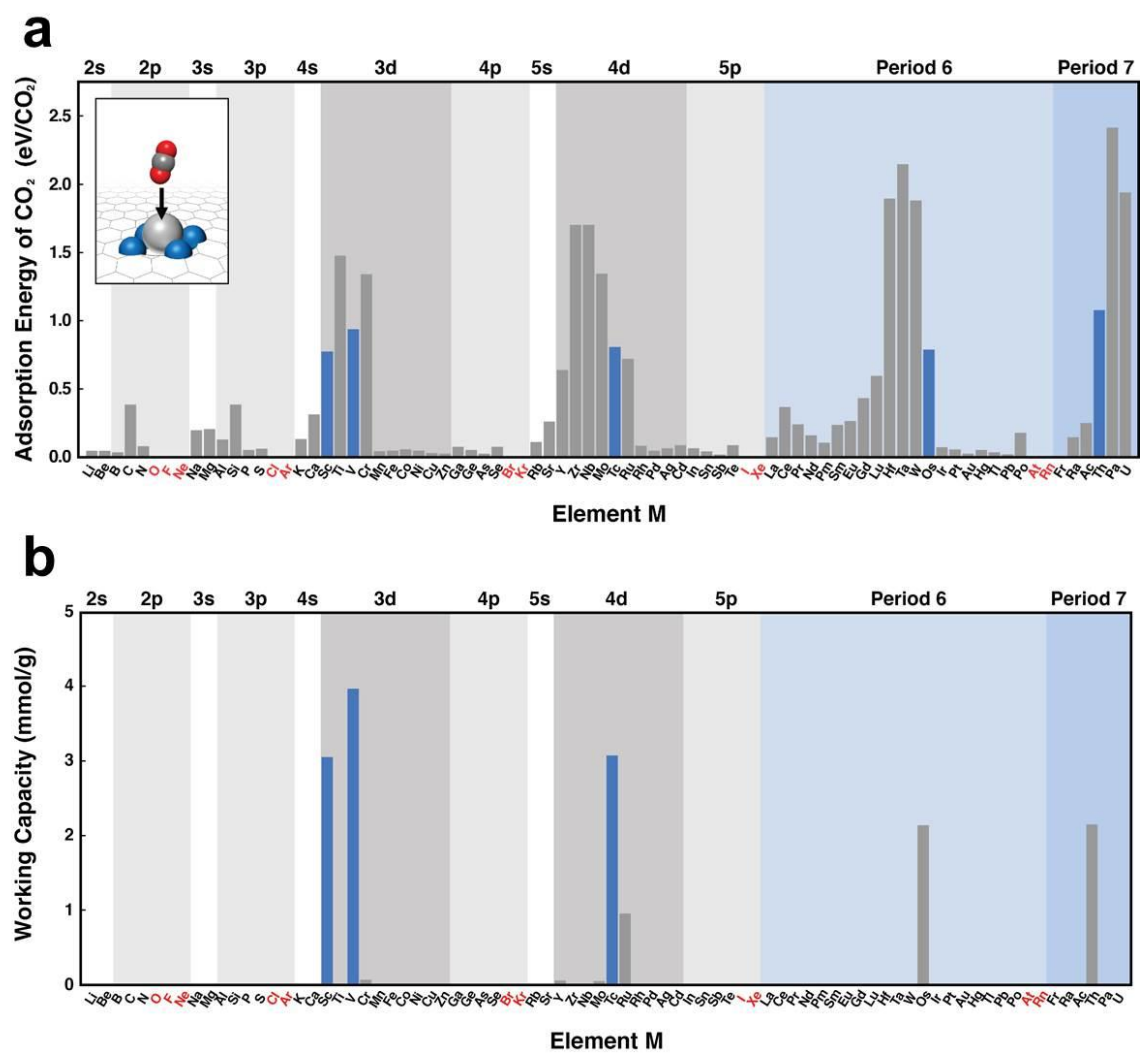
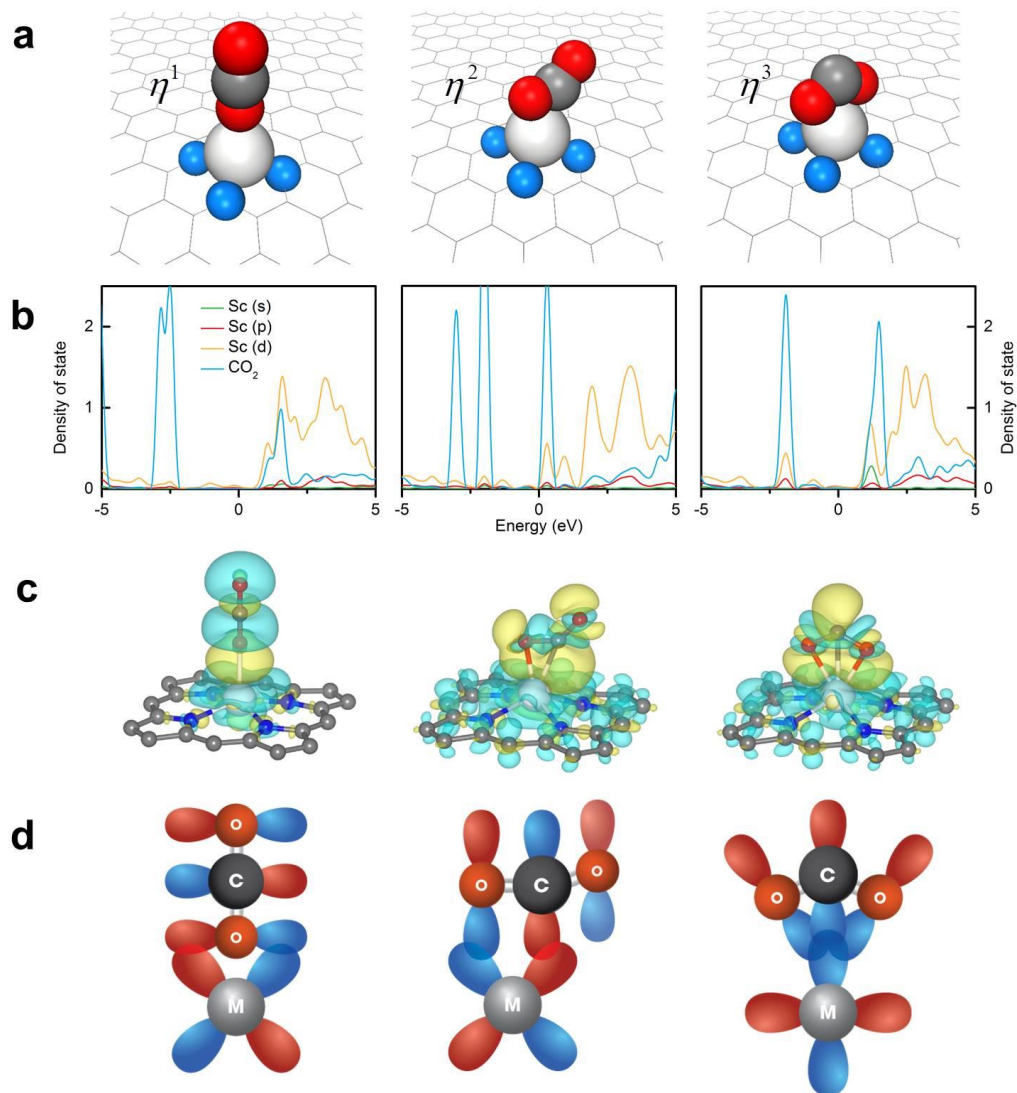


Figure 2



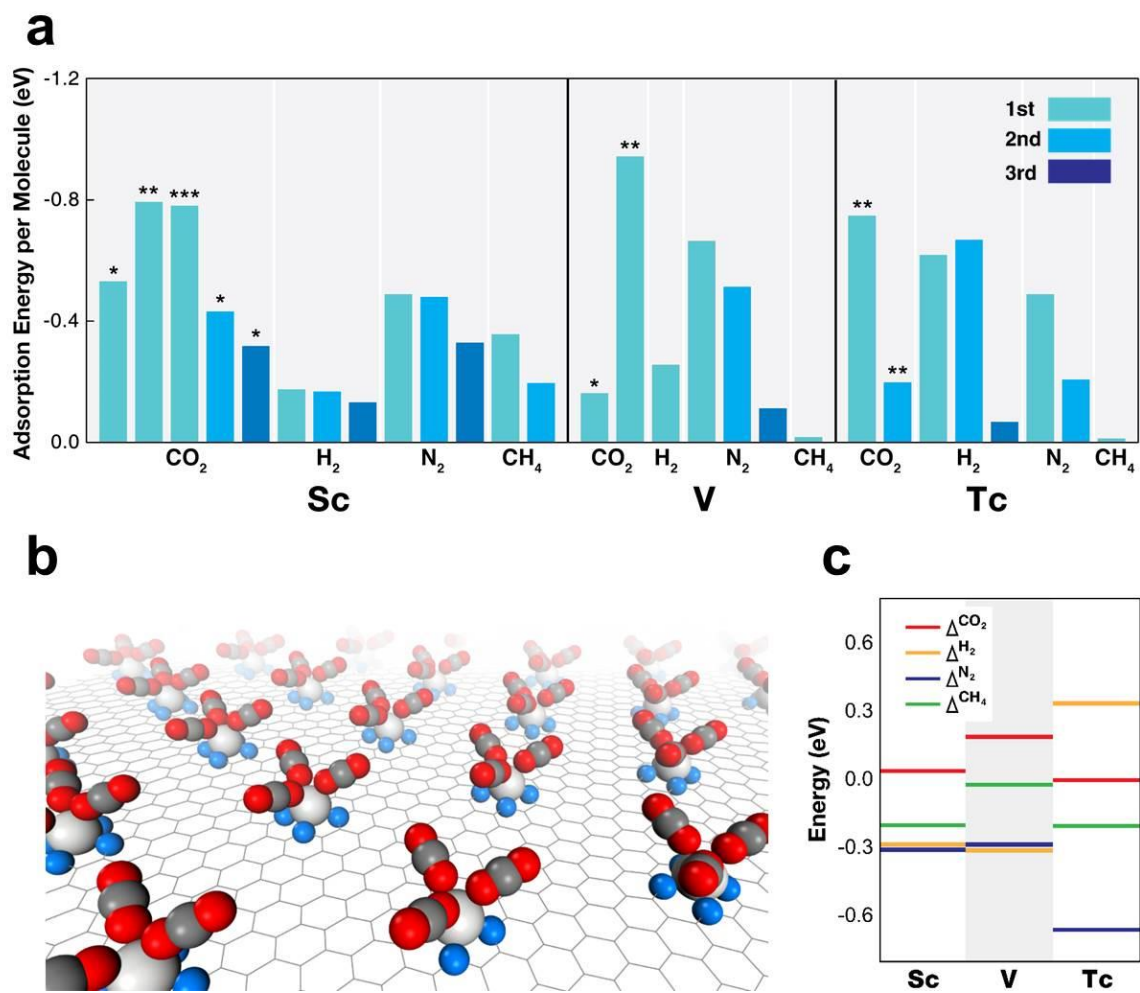


Figure 4

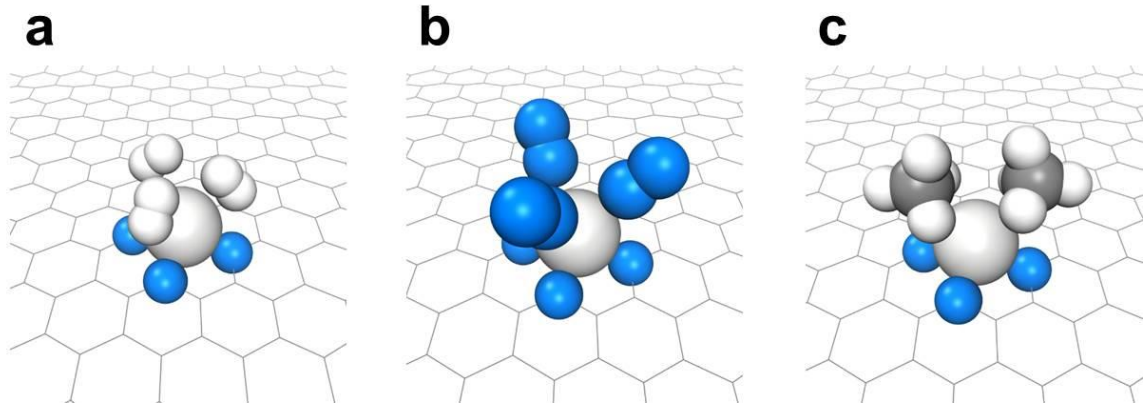


Figure 5

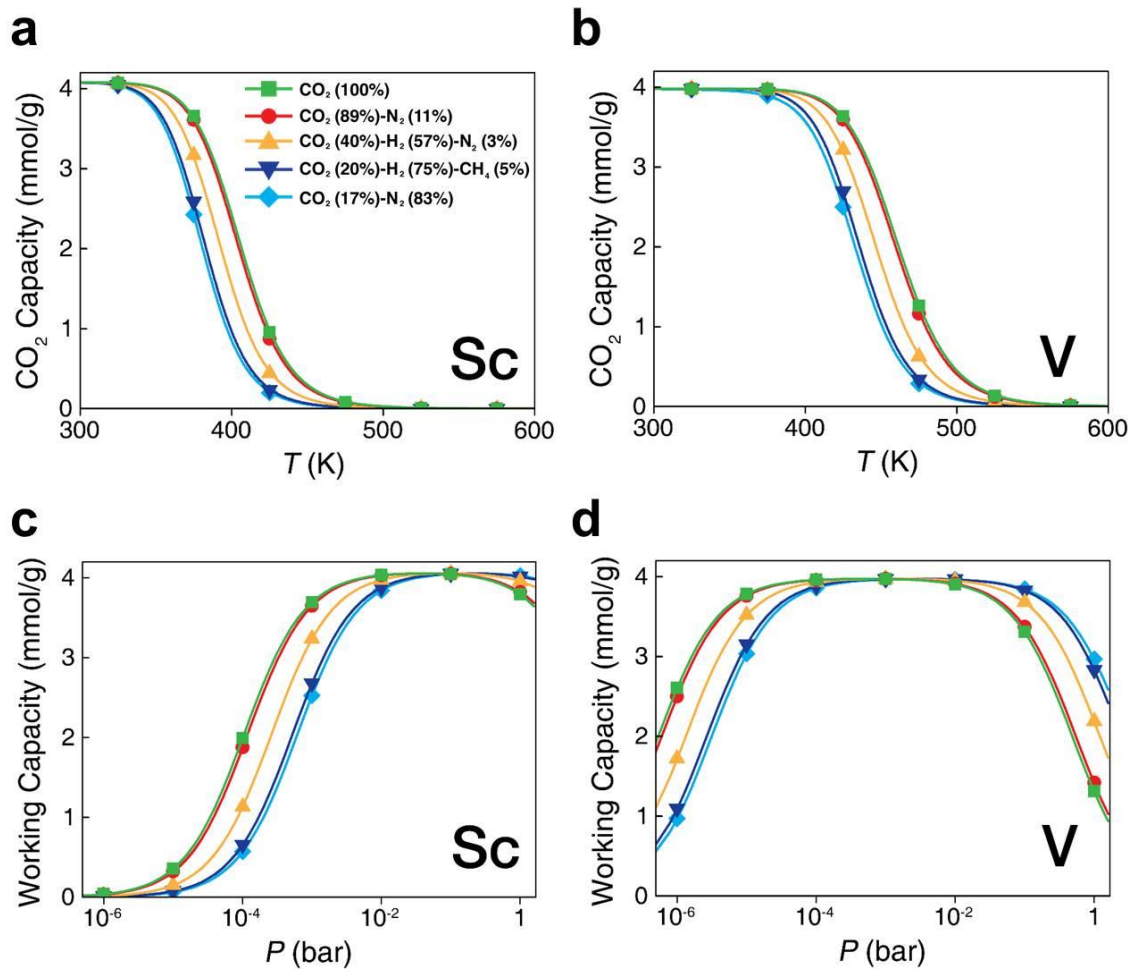


Figure 6